Alma Mater Studiorum · Università di Bologna

Scuola di Scienze
Dipartimento di Fisica e Astronomia
Corso di Laurea in Fisica

Scanning photoelectrochemical study of Cu_2O thin films coated by oxide and metallic overlayers

Relatore:
Prof. Luca Pasquini

Correlatore:
Marco Salvi

Presentata da:
Andrea Del Torchio

Anno Accademico 2023/2024

A Bologna,
alla mia famiglia,
ai miei amici (tranne Jack).
Alla Fortuna che mi è stata accanto.

Sommario

La crescente domanda mondiale di energia, unita all'obiettivo di mantenere la concetrazione atmosferica di CO_2 sotto le 450 ppm, crea l'esigenza di efficienti metodi di stoccagio dell'energia. A tal fine l'idrogeno è una soluzione attraente. I suoi processi di conversione in elettricità e di combustione sono già ben noti e attuabili, e presentano come sottoprodotto innocua H_2O.

Per la produzione di idrogeno l'uso dell'energia solare sarebbe ideale. Per questo scopo, le celle fotoelettrochimiche presentano un'alta efficienza teorica e una semplice struttura monolitica. Tra i possibili materiali per la realizzazione di fotocatodi, Cu_2O è facilmente ottenibile, non tossico, e presenta il band-gap appropriato.

In questo lavoro di tesi un fotocatodo di Cu_2O su SnO_2 dopato al fluoro (FTO) su vetro è stato modificato e studiato. Alcuni strati funzionalizzanti sono stati depositati sul campione e il loro ruolo è stato analizzato utilizzando un nuovo sistema ad alto rendimento. Nello specifico, sul campione sono stati depositati uno strato per il trasporto elettronico formato da ZnO dopato all'alluminio (AZO), uno strato di passivazione composto da TiO_2 e un catalizzatore sotto forma di nichel molibdeno. La caratterizzazione fotoelettrochimica del campione mostra che un'ottimizzazione ulteriore è richiesta per proteggere lo strato di Cu_2O dalla fotocorrosione e per migliorare il trasferimento elettronico dal fotocatodo all'elettrolita, il tutto preservando un trasporto elettronico efficiente fino alla superficie.

Abstract

The increasing global energy demand, coupled with the objective of keeping CO_2 atmospheric concentrations under 450 ppm, creates the need for efficient energy storage. For this purpose, hydrogen is an enticing choice. Hydrogen to electricity and combustion processes are already well studied and viable, with harmless H_2O as a byproduct.

To produce hydrogen the use of solar energy would be ideal. To this end, photoelectrochemical cells represent an option with theoretically high efficiency and a simple monolithic structure. Among all the materials for the realization of photocathodes, Cu_2O is widely available, non-toxic, and has the appropriate bandgap.

In this work, a Cu_2O on F-doped SnO_2 (FTO) on glass photocathode is modified and studied. Some functionalization layers were deposited on the sample and their role was studied by employing a novel high throughput setup and fabrication procedure. Specifically, an electron transport layer made of Al-doped ZnO (AZO), a passivation layer made of TiO_2, and a nickel molybdenum catalyst were added to the sample. The photoelectrochemical characterization shows that further optimization is needed in order to protect the Cu_2O film from photocorrosion and improve electron transfer from the photocathode to the electrolyte, while preserving an efficient electron transport efficiency to the surface.

Contents

Introduction

Among mankind's challenges during the twenty-first century, satisfying the global population's growing energy demand is one of primary importance. It is closely linked to another important challenge: getting the atmospheric carbon dioxide (CO_2) concentration under control. As of May 2024, the global atmospheric concentration of CO_2 has risen to 423 ppm, from the 280 ppm of the preindustrial level, with a current growth rate of 2.8 ppm/year [1]. A CO_2 level above 450 ppm carries a high risk of causing a change in global temperatures by more than 2 °C, according to the International Panel on Climate Change (IPCC). Such a change is projected to deeply impact the earth's ecosystems and human society [2, 3]. To tackle these challenges, the study and implementation of new types of energy storage will be of the utmost importance. Among all the options, hydrogen photo-generated through photoelectrochemical cells is especially palatable.

Source	Power Capacity (TW)
Wind	4
Hydroelectric	1-2
Tidal and ocean currents	< 2
Geothermal	12
Biomass	10
Nuclear	10
Solar	> 20

Table 1.1: Global energy capacity of sustainable energy sources. Note that these values are indicative and some remarks are to be made, as indicated in [5, 6]. For example, only a small fraction of geothermal energy can be exploited

1.1 Photoelectrochemically produced hydrogen as energy storage

1.1.1 The need for energy storage

The current reserves of fossil fuels are estimated to be sufficient to sustain an energy consumption of 25 to 30 TW for at least another century [4]. For this to be compatible with controlling CO_2 atmospheric concentration, carbon-capture technologies would need to be implemented on a scale not yet feasible. As shown in Table 1.1, among the various possibilities for sustainable energy resources solar appears to be the only capable of sustaining the world's entire energy consumption. A future energy infrastructure will rely on a mixture of all these sources, but it seems natural for solar to become the main contributor.

As the fraction of solar energy in the energy mix increases, the grid will have to cope with its intermittent nature (seasonal and daily cycles, cloud coverage). In this regard, chemical fuels present high energy densities and ease of transportation, making them a sensible candidate for energy storage.

1.1.2 The case for hydrogen

Among chemical fuels, most require a source of carbon to be synthesized. Some examples are methane, methanol, and gasoline. Atmospheric CO_2 is an obvious candidate as a source of carbon, but the high entropic cost of its retrieval due to its low concentration in air makes for a bad match. Other retrieval options include extraction from high-concentration fumes in power plants or vehicles, thus closing the CO_2 loop. Even if the energetic penalty coming from carbon dioxide extraction comes to be addressed, the direct photochemical conversion of CO_2 to a fuel remains challenging, as it involves six- or eight-electron transfer steps, depending on the fuel.

In this context, the conversion of solar energy to hydrogen seems more promising. Hydrogen is present in water, which is abundant and convenient. The water-splitting reaction can be written as:

$$2\,H_2O + h\nu \rightleftharpoons 2\,H_2 + O_2 \tag{1.1}$$

Here the reduction half-reaction is a two-electron transfer, while the oxidation half-reaction requires a four-electron transfer (reactions indicated in an alkaline environment):

$$\begin{aligned} 2\,H_2O + 2\,e^- &\longrightarrow 2\,H_2 + OH^- \\ 4\,OH^- + 4\,h^+ &\longrightarrow 2\,H_2O + O_2 \end{aligned} \tag{1.2}$$

By no means trivial, these reactions are considerably easier to achieve than the photo-reduction of CO_2.

One of the main advantages of choosing hydrogen as the fuel of preference resides in its ability to be easily converted to electricity through fuel cells and electrolyzers. Another advantage is the already high demand for hydrogen at the global scale. Hydrogen is a necessary molecule for the production of ammonia, NH_3. Ammonia is an extremely useful substance in the chemical industry, most notably due to its role as a fertilizer. The global demand for ammonia reached 170 million tons in 2022 and is expected to keep growing [7]. Hydrogen finds use also as a coolant, as a high-temperature fuel in industrial settings, as a rocket propellant, and more. In 2022, 70 % of hydrogen production came from natural gas through the process of steam reforming ("gray" hydrogen), while 20 % came from coal ("black" hydrogen) [8]. Both of these processes emit greenhouse gasses as byproducts, so their phase-out in favor of "clean" hydrogen production has to be accomplished to meet the aforementioned energy targets.

One concern related to a hydrogen-oriented energy infrastructure is the storage difficulty. While having one of the highest gravimetric energy densities, hydrogen has one of the lowest volumetric energy densities among the chemical fuels. This is of course because at room temperature and pressure, hydrogen takes gaseous form. Solutions to this problem include liquid cryo-storage, high-pressure storage, metal hydrides, physisorption with metal-organic frameworks (MOFs), and using hydrogen and CO_2 to make carbon-based fuels [9].

1.1.3 Water splitting techniques

The conversion of water and energy to hydrogen can be achieved in many different ways, some are:

- Electrolysis systems
- Molecular artificial photosynthesis
- Magnetolysis
- Plasma-chemical conversion
- Photoelectrochemical (PEC) water splitting
- Photocatalytic water splitting
- Photobiological methods
- Thermochemical conversion

Most of these do not rely directly on the sun, requiring an external power source. Thanks to the introduction of photovoltaic methods, many of them can be turned into solar-water to hydrogen processes.

As will be shown in the following sections, electrolysis and photoelectrochemical water splitting offer the advantage of producing hydrogen and oxygen at separate electrodes. This relieves various safety concerns and prevents costly post-separation of the gasses. They can also be carried out at room temperature and are usually constructed out of inorganic materials, making for chemically robust systems, something hard to achieve with organic compounds.

The photovoltaic-electrolysis system's components are all commercially available: solar cell, electrolyzer, dc-dc converter. Solar-to-hydrogen efficiencies for such systems have been demonstrated to reach 12-18% [10], which can be considered a benchmark for photoelectrochemical systems.

PEC systems present the great advantage of reduced complexity over photovoltaic-electrolyzers. A PEC system produced on a large scale is potentially cheaper and faster to build, being made of a single component with fewer materials and no need for later assembly [11].

It must be pointed out that current photovoltaic-electrolyzer systems far outperform PECs, and that this technology is already commercially available, even though pilot experimental plants present a cost per kilogram of hydrogen still higher than the 2$ threshold indicated by the U.S. Department of Energy for 2026[12] (this value was developed with stakeholder input to enable competitiveness with incumbent and emerging technologies) .

Seeing the potential advantages of PEC systems, their study is worth the time and effort, and their performance is to be compared with current photovoltaic-electrolysis systems.

1.2 Introduction to electrochemistry

An electrochemical cell is a device that generates electrical energy from chemical reactions, or that uses it to drive a reaction. An in-depth analysis of electrochemical techniques is given in [13, 14]. In this section, the main points are summarized.

1.2.1 REDOX reactions and conventions

REDOX reactions set the basis of electrochemistry. These are reactions involving the exchange of electrons among chemical species. When a species gains an electron, its oxidation number diminishes, the species is then said to be *reduced*. On the opposite side, when one species loses an electron it is said to be *oxidized* . In electrochemistry, these reactions are studied by placing in contact a solid metal *electrode* with a liquid phase (*electrolyte*). These form a *half-cell*, it too called "electrode". Two electrodes separated by a porous septum form a cell.

The physical principle at the base of their study is the different *affinity* of each material's particles (in our treatment electrons) to a different material. When different materials are put in contact, this difference in affinity may cause some particles to migrate from one to another, giving rise to measurable physical effects. The physical intuition for this phenomenon may be aided by the use of "chemical forces". By

imagining the forces acting on a particle at the interface between the two materials, their sum may be different from zero, causing the particle to move and cross the interface. The presence of such a net force may instead be interpreted as the presence of a potential difference at the interface, causing the movement of particles. Particles are then exchanged until the potential in each material reaches the same value.

A complete theoretical treatment of this phenomenon has not yet been achieved, as it would have to take into account all the different interactions between particles. Assigning a value to this potential difference carries various considerations. For example, the measure of such contact potential would introduce, through the instrument, new contact potential. A potential is also not an absolute value. It must be indicated in reference to a well-defined system. From this, the need for *reference electrodes* arises. Of course, the choice of the particular reference electrode is arbitrary. Commonly used reference electrodes are the Standard Hydrogen Electrode (SHE) and the Normal Hydrogen Electrode (NHE).

1.2.2 Nernst's equation

Through classical thermodynamics, the dependence of such a potential difference from physical parameters may be obtained. The spontaneity of a chemical reaction is, at constant pressure and temperature (as is usual in electrochemical systems), indicated by Gibb's free energy $G = U + pV - TS$ where U is internal energy, p is pressure, V is volume, T is temperature, and S is entropy. Processes in which Gibb's free energy decreases are spontaneous. At equilibrium the energy is minimal, and the equilibrium condition can be expressed as $dG = 0$. Gibb's free energy is an additive function. For systems made of pure components $G = \sum_k n_k G_k$ where G_k is the specific Gibbs energy of components k (e.g. J/mol) and n_k is the quantity of component k in the system (moles).

For small changes in the composition of such systems, one has

$$dG = \sum_k \frac{\partial G_k}{\partial n_k} dn_k = \sum_k \mu_k dn_k$$

where the parameter $\mu_k = \frac{\partial G_k}{\partial n_k}$ is called *chemical potential* of the component k (of course the partial derivatives keep all other parameters constant).

For an ideal gas one finds $\mu_k = \mu_k^0 + RT \ln p_k/p_0$, having set p_k as the partial pressure of the gaseous species k and p_o is a reference pressure. For sufficiently diluted solutions a similar formula is found:

$$\mu_k = \mu_k^0 + RT \ln c_k/c_0 \tag{1.3}$$

where c_k is the concentration of the component k, c_0 is a reference concentration, and μ_k^0 is a parameter called *standard chemical potential*. This parameter represents the chemical potential of the system in the reference state. Solutions that obey this formula are similarly called ideal solutions.

When treating ions, their energy does not only depend on the chemical forces but also on the presence of an electric field. In the case of an electrostatic field given by the potential Ψ, one defines the *electrochemical potential* of an ion as its chemical potential plus its electrostatic potential energy:

$$\bar{\mu}_k = \mu_k + z_k F \Psi \tag{1.4}$$

Where z_k is the charge number and F is the Faraday constant, given by the elementary charge times Avogadro's number. This definition assumes that a change in concentration would affect only μ_k, while only the second term would be affected by a change in potential. This is an approximation, as a change in ion concentration means a change in charge and so in potential. In most cases, a change in potential is associated with concentration changes so small that the concentration can for all practical purposes be regarded as constant. At equilibrium, the electrochemical potential represents the thermodynamic work to add one ion to the system. This is the definition of the potential introduced in the previous paragraphs. In solid-state physics, it is usually referred to as *Fermi level*, terminology that will be adopted from here on.

When straying from ideal solutions, the convention is to keep the form of Eq. 1.3 by substituting the concentration c_k with a parameter called *activity* (indicated by a_k for the component k). Note that the constant μ_k^0 is not a priori the same, but it is taken to be by assuming that for highly diluted concentrations $\lim_{c_k \to 0} a_k = c_k$. Activity is taken to be unitary for liquid and solid phases of a single component.

For reactions of the type

$$\sum_{j \in Ox} \alpha_j X_j + n e^- \rightleftarrows \sum_{i \in Red} \alpha_i X_i$$

where α are the stoichiometric coefficients of the species, one finds the change in Gibb's free energy to be:

$$\pm \Delta G = (\sum_{j \in Ox} \alpha_j \bar{\mu}_j + n \bar{\mu}_e) \Delta n_{Ox} + (\sum_{i \in Red} \alpha_i \bar{\mu}_i) \Delta n_{Red} \tag{1.5}$$

Having set Δn as the moles of a hypothetical component with stoichiometric number $\alpha = 1$ taking part in the reaction. The $\pm$ sign is to differentiate the anodic $(+)$ and cathodic $(-)$ reactions (we will take anodic reactions from now on). In this equation Δn_{Ox} is related to Δn_{Red} through $\Delta n_{Ox} = -\Delta n_{Red}$ since the oxidation of a mole of material implies the creation of a mole of reduced material (if both have a stoichiometric coefficient of 1 as defined). Introducing the equilibrium condition $(\Delta G = 0)$ and using Equation 1.4 the following is obtained:

$$(\sum_{j \in Ox} \alpha_j (\mu_j + z_j F V_{sol}) + n(\mu_e + F V_{el}) - \sum_{i \in Red} \alpha_i (\mu_i + z_i F V_{sol})) \Delta n_{Red} = 0 \tag{1.6}$$

Here V_{sol} is the value of the potential in solution (where the reacting ions are situated), and V_{el} is the potential in the electrode (felt by the electrons). Once again not all the variables are independent. The conservation of charge requires that:

$$\sum_{j \in Ox} \alpha_j z_j - \sum_{i \in Red} \alpha_i z_i + n = 0 \tag{1.7}$$

By inserting 1.7 in Equation 1.6, dividing by Δn_{Red} and rearranging the terms:

$$nF(V_{sol} - V_{el}) = \sum_{i \in Red} \alpha_i \mu_i - \sum_{j \in Ox} \alpha_j \mu_j - n\mu_e$$

As discussed above it is now possible to use equation 1.3 for non-ideal systems (by using the activity parameter) to substitute the chemical potentials:

$$nF(V_{sol} - V_{el}) = (\sum_{i \in Red} \mu_i^0 - \sum_{j \in Ox} \alpha_j \mu_j^0 - n\mu_e) + RT(\sum_{j \in Ox} \alpha_j \ln a_j - \sum_{i \in Red} \alpha_i \ln a_i)$$

The first term in brackets on the right-hand side is the standard molar Gibb's free energy of the reaction ΔG_0. Diving by the constant term on the left Nernst's equation is obtained:

$$\Delta V = V_0 + \frac{RT}{nF}(\sum_{j \in Ox} \nu_j \ln a_j - \sum_{i \in Red} \nu_i \ln a_i) \tag{1.8}$$

Where $\Delta V = V_{sol} - V_{el}$, and V_0 is the *standard reduction potential*, given by

$$V_0 = \frac{\sum_{i \in Red} \mu_i^0 - \sum_{j \in Ox} \alpha_j \mu_j^0 - n\mu_e}{nF} = \frac{\Delta G_0}{nF}$$

.

Nernst's formula relates the potential difference of an electrode-electrolyte system to the component's activities.

1.3 Photoelectrochemistry

A photoelectrochemical cell is based on the junction between a semiconductor (*working-electrode*) and an electrolyte (normally liquid), containing a suitable redox couple. The main element of the system is the semiconductor. Here the incident photons are transformed into electron-hole pairs, subsequently separated due to the presence of an internal electric field. For the simplest PEC, the semiconductor is connected (through the *back-contact*) to a *counter-electrode*. Two schematic cells, one with the semiconductor as photoanode and one as photocathode, are shown in Figure 1.1

1.3.1 Band structure

Solid-state physics is the branch of physics that deals with the description of systems in the solid state of matter, especially crystalline ones. The problem of finding the energy levels of the electrons in a solid is translated into the solving of Schrödinger's equation for the system of nuclei and electrons. In crystalline solids, this approach can be undertaken directly. A crystalline solid is one described by three vectors, $\vec{a}$, $\vec{b}$, and $\vec{c}$, such that the solid's structure is invariant under translations of an integer linear combination of these vectors: $\vec{R} = m\vec{a} + n\vec{b} + o\vec{c}$. Since the atoms in the lattice create the internal electric potential, this one must also satisfy the translation invariance property. Thanks to this invariance property an important theorem can be used: Bloch's theorem. It states that if the potential is periodic

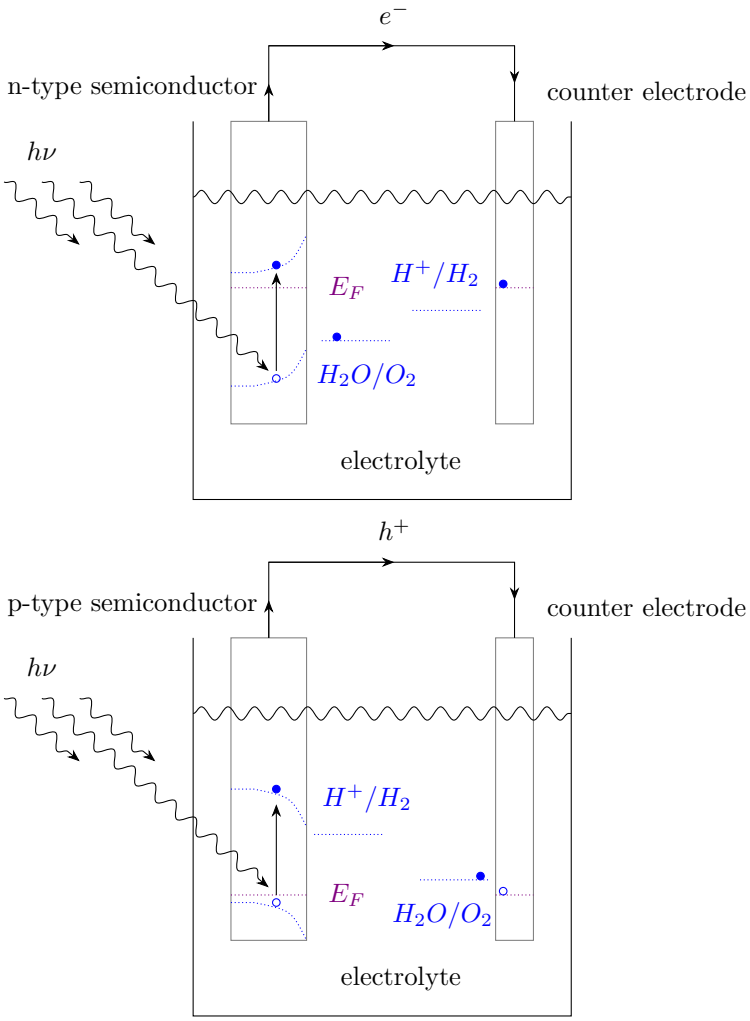

Figure 1.1: *Example of 2-electrodes photoelectrochemical cells. On the top a n-type semiconductor functioning as a photoanode, and on the bottom a p-type semiconductor, as a photocathode. In blue are indicated the energy bands of the semiconductor and the oxidation/reduction potentials of water. In violet, the Fermi level is indicated. Empty circles represent holes, while full circles represent electrons*

in space (invariant under translation) the solutions for Schrödinger's equation of a single electron:

$$[-\frac{h^2}{2\pi^2}\nabla^2 + V(\vec{r})]\psi_k(\vec{r}) = E_k\psi_k(\vec{r})$$

are given in the form $\psi_k = e^{i\vec{k}\vec{r}}U_k(\vec{r})$, where $U_k(\vec{r})$ is itself periodic in $\vec{r}$ with the same periodicity of the lattice. In these formulas h is Planck's constant, $\vec{r}$ is the position in the lattice (referencing a determined and stationary frame relative to the lattice), $V(\vec{r})$ is the electric potential, $\vec{k}$ is the electron's wave vector used to index the solutions, E_k are the electron's possible energy levels, and $\psi_k(\vec{r})$ is the electron's wave function.

This equation can be solved (most often approximated through numerical methods) when an explicit potential is given. It results in a eigenvalue problem with infinite solutions, thus obtaining infinite possible energy levels for each value of k. These infinite levels may be indexed by other quantum numbers $\vec{n}$, in which case the reasoning can be inverted, and the energy levels can be though of as indexed by k for each quantum number multiplet $\vec{n}$. In the limit of an infinite lattice k varies continuously, and the energy levels form energy *bands*. When electrons are then "placed" in these bands, starting from lower to higher energy respecting Pauli's exclusion principle, the position of the last electron defines the character of the material. If its energy level is situated in the middle of an energy band (thus having unoccupied higher energy states in the same band), the material is a conductor (metal). If the energy level of the electron is the last allowed for the band (thus the band is "full"), the material is either a semiconductor or an insulator, depending on the energy distance from the next "free" energy band. In this case the last filled band is called *valence* band, while the first empty band is called conduction band. The "energy distance" between bands is called *bandgap*, and its defined as the difference between the lowest energy of the conduction band E_C minus the highest energy of the valence band E_V.

By studying the electronic bands structure's dependence on the wave vector many insights on a material's behaviour may be gained. First of all, if the lowest point of the conduction band is situated at the same k-vector as the highest point of the valence band, then a transition between these two points is called *direct*. Such a transition does not require a change in crystal momentum and is thus favored when compared to an *indirect* transition, where the two bands' edges happen at a different k. In this second kind of transition, the momentum of the electron needs to change. Photons carry too little momentum, so instead the required amount has to be provided by something else. Usually, the crystalline lattice vibrations can provide the required momentum, as the atoms interact with the electron. In solid-state physics, this kind of interaction is described with the creation or annihilation of a *phonon* (a quantum of energy of a normal mode of vibration of the crystal lattice). The need for the simultaneous absorption of a photon and absorption or emission of a phonon makes the process less likely, and thus the light absorption coefficient for indirect semiconductors is much smaller than that of direct semiconductors.

A second piece of information that one can obtain from the E-k diagram is the mobility of charge carriers. In fact, the effective mass m^* of a charge carrier can be computed as:

$$m^* = \frac{h^2}{\frac{\partial^2 E}{\partial k^2}}$$

where h is Planck's constant. The carrier's mobility μ is given by the relation $\mu = \frac{q\tau}{m^*}$, where q is the charge of the carrier and τ is the average time between one scattering event and the following one. This has the direct interpretation that *strongly curved bands indicate a high charge mobility* (together with the width of the band).

A third piece of information one can obtain from an E-k diagram is the density-of-state (DOS) of the system. This represents the number of allowed states as a function of the energy.

Using these tools it is possible to check, for example, how the intrinsic charge carriers mobility is very low for metal oxide semiconductors. As will be discussed further in Section 1.4, this is not ideal. The conductivity σ of a material (where electrons and holes are the charge carriers) is given by $\sigma = ne\mu_e + pe\mu_p$, where μ_n, n, μ_p and p are the mobility and concentration of electrons and *holes*, respectively. Holes are vacancies in the electron sites of the crystalline structure, which may be filled by neighboring electrons, effectively "moving" the hole. A quantum-mechanical treatment of this process shows that it is equivalent to the movement of a fictitious particle of mobility μ_p.

Doping is a common method to increase the conductivity of these materials. This is the process of introducing impurities in the structure to increase the number of charge carriers. Grossly speaking, donor atoms have loosely bound electrons, which are able to "make the jump" to the conduction band thanks to thermal agitation, thus increasing conductivity. Materials with this type of doping are referred to as n-type. On the opposite side, acceptor atoms have an electron vacancy in their electronic shell, thus "accepting" electrons from neighboring atoms. This creates a hole, which, as shown earlier, behaves as a positive charge carrier. Materials doped in this way are called p-type.

1.3.2 The space charge layer

As introduced in the previous section, when two materials having different potential levels (Fermi levels) for charge carriers come in contact, charges are exchanged between them until equilibrium is reached. In the case of metal oxides, water molecules from the air may adsorb at the surface, resulting in surface OH^- groups. These groups create electronic states within the bandgap of the semiconductor. Electrons from the bulk of the material then occupy these states, leaving behind ionized donors. This creates an electric field which increases until equilibrium is reached. The potential distribution and space charge width are useful for a quantitative study of photoelectrochemical cells.

Poisson's law states $\frac{d^2\phi}{dx^2} = \frac{-\rho(x)}{\epsilon_0 \epsilon_r}$, where $\phi(x)$ is the potential, $\rho(x)$ is the charge density, and $\epsilon_0 \epsilon_r$ are the dielectric constant of vacuum and the relative dielectric constant of the medium, respectively. In the case of an n-type material (a similar treatment may be followed for p-type materials), the charge density is given by

$$\rho(x) = e(N_D^+ - n(x))$$

where N_D^+ is the ionized donor's atoms concentration and $n(x)$ is the concentration of free electrons. This depends on the band minimum and the Fermi level: $n(x) = N_c e^{-(E_C - E_F - e\phi(x))/kT} = n_b e^{e\phi(x))/kT}$. Here k is Boltzmann's constant and n_b is the density of free electrons in the bulk (where no electric field "bends" the energy band). The resulting coupled equations cannot be solved directly.

To do so one takes the derivative of the square of the electric field ξ:

$$\frac{d(\xi^2)}{dx} = 2\xi\frac{d\xi}{dx} = -2\frac{\rho(x)}{\epsilon_0\epsilon_r}\frac{d\phi}{dx}$$

By combining this with Gauss's law $\xi = Q/\epsilon_0\epsilon_r A$ with the approximation that $N_D^+ = N_D = n_b$, the following may be obtained:

$$Q = \sqrt{2\epsilon_0\epsilon_r e N_D A^2(\phi + \frac{kT}{e}e^{-e\phi/kT} - \frac{kT}{e})} \simeq \sqrt{2\epsilon_0\epsilon_r e N_D A^2(\phi - \frac{kT}{e})}$$

Here the term $\frac{kT}{e}e^{-e\phi/kT}$ is removed since typical values of ϕ exceed 0.1 V, while at room temperature kT is about 26 meV

The width of the space charge layer is thus found via $Q = eN_d AW$:

$$W = \sqrt{\frac{2\epsilon_0\epsilon_r}{eN_D}(\phi - \frac{kT}{e})}$$

The previous also allows for the determination of the space charge layer differential capacitance C_{SC}:

$$\frac{1}{C_{CS}^2} = (\frac{dQ}{d\phi})^{-2} = \frac{2}{\epsilon_0\epsilon_r e N_D A^2}(\phi - \frac{kT}{e}) \tag{1.9}$$

This is the so-called Mott-Schottky equation. By plotting the capacitance in function of the applied potential it is possible to obtain physical parameters like the value of the doping of the material.

1.3.3 Surface Hydroxylation

The last section treated the formation of a space charge layer in a metal oxide semiconductor exposed to air. A slightly different treatment is needed when said semiconductor is in contact with an electrolyte solution, as in most PEC cells.

Similarly to what was discussed for semiconductor-air interfaces, in aqueous solutions there is continuous adsorption and desorption of molecules. The main contributors are H^+ and OH^- ions, adsorbing and desorping over the surface of the semiconductor. A dynamic equilibrium is reached eventually between the desorption $M{-}OH \xrightleftarrows{k_a} MO^- + H^+$ and adsorption $M{-}OH + H^+ \xrightleftarrows{k_b} M{-}OH_2{}^+$. The pH at which, at equilibrium, the net adsorbed charge is zero is called the zero point charge (PZC). The adsorbed ions form a layer with a net charge called *inner Helmholtz layer*. The net charge created due to this reaction has to be compensated inside the semiconductor, creating an electric field.

In water, especially when treating electrochemical cells, the presence of REDOX species also contributes to the exchange of electrons between the semiconductor and the solution, as illustrated in Section 1.2. Once equilibrium is reached, a further

charge imbalance is created, accentuating the band bending and leaving ions in the solution. Due to the strong polarity of water, these ions will be surrounded by a cloud of water molecules, preventing them from approaching the semiconductor's surface as in the case of the inner Helmholtz layer. This creates a new layer of charges at a distance dictated by their solvation volume, called the *outer Helmholtz layer*.

The voltage difference across such a layer is given by $V_H = \xi d = Qd/\epsilon_0\epsilon_r$, where d is the width of the Helmholtz layer. By studying the equilibrium constants at $pH = PZC$ it is possible to obtain the value for the voltage drop across the Helmholtz layer:

$$V_H = \frac{2.3kT}{e}[(\log\frac{[M-O^-]}{[M-OH_2^+]})^{\frac{1}{2}} + PZC - pH]$$

The excess charge at the surface is usually very small, so $[M-O^-] \simeq [M-OH_2^+]$, obtaining the simplified equation:

$$V_H = \frac{2.3kT}{e}(PZC - pH) \tag{1.10}$$

which corresponds to a potential drop of $-59\,\mathrm{mV}$ per unit pH at $25\,^\circ\mathrm{C}$.

1.3.4 PEC cell energy diagram

An example energy diagram for an n-type semiconductor and metal counter electrode is shown in Fig. 1.2. The parameters of interest are the amount of band bending, the band positions, and the difference between E_F and E_C.

This diagram shows directly if a certain reduction/oxidation reaction is possible. In the case of oxidation, when a photon hits the semiconductor it may excite an electron from the valence to the conduction band, thus creating an electron-hole pair. The hole will be at the energy level E_V, and will "climb" the energy band towards the interface. This allows electrons from the redox species' oxidation reaction to enter the semiconductor. For the reaction to occur the final energy of the redox species' electron must be lower than the redox energy of the reaction. In the diagram, this means that the redox energy of the H_2O/O_2 redox couple must be *higher* than the energy band at the interface.

The operation of the cell may be influenced by applying an external bias potential to the working electrode (a potential relative to a reference point, or better the *reference electrode*, whose role will be discussed later). The potential drop must be localized in the space charge region and Helmholtz layer. Since both layers have the same amount of charge Q accumulated, the potential distribution will be given by

$$\frac{\Delta V_{SC}}{\Delta V_H} = \frac{C_H}{C_{SC}}$$

Since usually $C_H \gg C_{SC}$, the potential loss happens predominantly in the space-charge region. This allows the control of band bending in the semiconductor.

To further control the oxidation/reduction capacity of a semiconductor it also seems natural to use the dependence on pH of the Helmholtz potential as seen in Eq. 1.10. For example by using more acidic solutions one would be able to increase V_H,

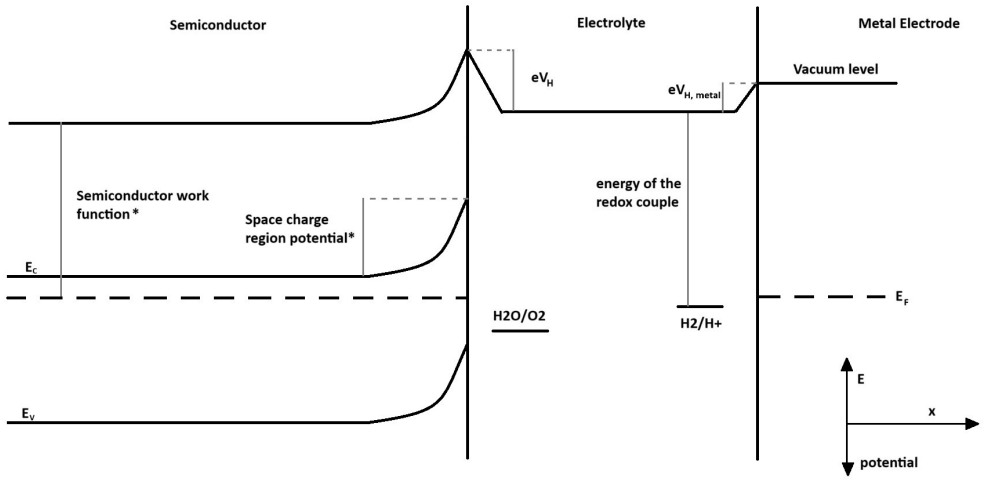

Figure 1.2: *Energy diagram of a PEC cell based on a n-type semiconductor and metal electrode. The asterisc indicates that the indicated variable is a potential, and thus must be multiplied by the charge of the charge carrier to be represented as energy. Note that the Helmholtz layer is also present at the metal/electrolyte interface*

thus lowering E_C and E_V, increasing the oxidation power of the cell while simultaneously lowering its reduction capacity. Unfortunately, this gives no advantage when it comes to water splitting due to the dependence of water's reduction/oxidation potentials on the pH via Nernst's reaction 1.8. This gives (for most metal-oxides) the same $-59\,\mathrm{mV}$ per unit pH dependence as the band edge, making the relative distance of the band edges and oxidation potential of water fixed.

Another important parameter when studying PEC cells is the *flatband* potential. This is defined as the bias potential needed to flatten the band bending. It indicates the position of the Fermi level of the semiconductor in relation to the reference potential (taken to be that of the earlier defined SHE). It accurately reflects the capacity of an n-type semiconductor to reduce water to hydrogen.

1.4 Material choice for PEC cells

The choice of photoanode/photocathode material is one of the most crucial parts of constructing a viable PEC cell. Some requirements on the materials seem to be in conflict, and trade-offs have to be made.

1.4.1 Required characteristics for a PEC cell

The required characteristics for a suitable material may be summarized as follows:

1. Band edge position straddling the oxidation and reduction potentials of water
2. Good light absorption (in the sun spectrum)
3. Low overpotentials

4. High chemical stability

5. Efficient charge transport in the semiconductor

6. Low cost

The band edge requirement comes naturally from the necessity of having the valence band level below the oxidation potential of water and the conduction band level above the reduction potential of water. This band edge requirement also impacts the bandgap and thus the light wavelengths with a sufficiently high absorption coefficient. The higher the bandgap, the higher the photon's energy required for a band to band transition.

The requirement for chemical stability is a simple one but is most often problematic to satisfy. Many candidate materials are vulnerable to processes such as oxidation and photocorrosion, which limit their lifetime.

The minimization of the over-potential comes from the goal of reaching *efficient* water splitting. Any energy difference between the required energy by the reaction and the energy gap of the semiconductor will be lost to other forms of energy (e.g. heat). Since the excitation of the electron comes from the photon, this means that a lower hydrogen yield is reached with light of the same energy.

Efficient charge transport is required for low recombination of charges. When the electro-hole pair is created in the semiconductor, they start moving in opposite directions due to the electric field present. To prevent the majority of the carriers from recombining (and thus losing the absorbed energy from the photon) they have to spend in the semiconductor a time comparable to their recombination time.

Low cost is required to implement the technology on a commercial scale.

1.4.2 Relevant physical parameters

The minimum bandgap is given by the energy requirement for water splitting: 1.23 eV. Thermodynamic losses also have to be accounted for, which usually account for around 0.3 to 0.4 eV. By adding to these the overpotentials needed for fast reaction kinetics the optimal bandgap is found, amounting at 1.9 to 2.1 eV [15, 16]. An upper bound to the bandgap might be assigned by noting that the intensity of light drops sharply below 400 nm, giving a value of 3.1 eV. Band edge tables also convey information regarding the overpotentials.

When analyzing the chemical stability requirement, it can be noted how most non-oxides dissolve or form a thin oxide layer. Semiconductor oxides are chemically more stable but may be prone to photocorrosion. A wider band gap is generally associated with higher resistance to photocorrosion [17].

The requirement for efficient charge transport is illustrated by the carrier's lifetime τ_R, or by the minority carrier's diffusion length, given by $L_D \simeq \sqrt{D\tau_R}$ where D is the diffusivity of the free carriers, related to their mobility by the Nernst-Einstein equation:

$$D = \frac{kT\mu}{e}$$

This length is to be compared to the distance traveled by the charges to reach the interface. Information regarding the charge transport may be extracted by the

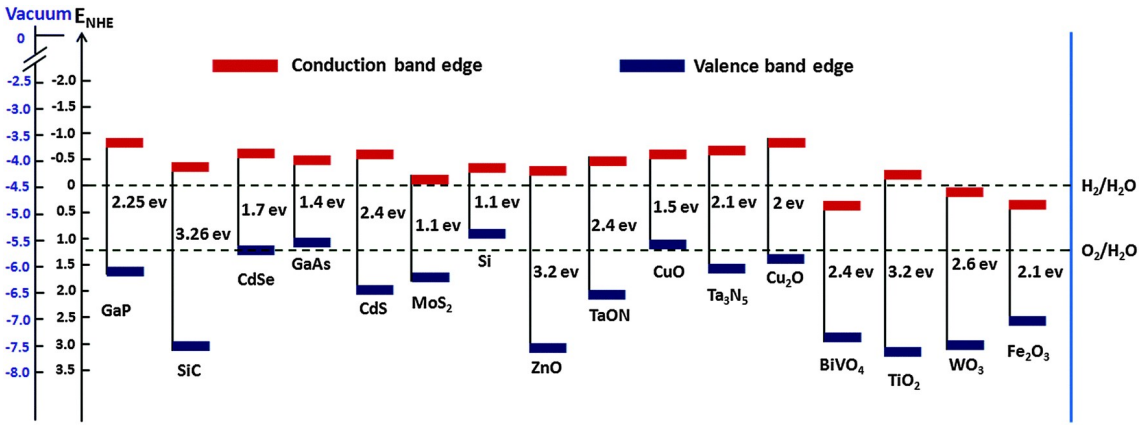

Figure 1.3: *Band edge positions of semiconductors in contact with the aqueous electrolyte at pH = 0 relative to NHE and the vacuum level. Reproduced from Ref. [18] with permission from the Royal Society of Chemistry.*

material's electronic band structure. Usually, high electron mobility is associated with extensive metal 3d orbitals overlap, while O-2p orbitals overlap indicates increased hole mobility in metal oxides. Other factors like recombination centers and the presence of shallow (i.e. with energy levels near the conduction/valence band) donors/acceptors have also a marked importance. This is especially true in the case of catalyst, which may increase recombination rates through lowered mobility or by introducing recombination centers.

It is thus possible to identify four trade-offs:

- The need for small overpotentials against increased stability at higher bandgaps
- Increased reaction driving force at higher bandgaps against a reduced ability of solar light to excite electrons
- The minimization of recombination sites opposed to the need for catalysts
- Performance versus cost

At present, no one perfect material has been found, but many have been analyzed. In the next subsection, some materials are presented and an overview of the methodologies used to address the different material's limitations is given.

1.4.3 Choice of materials and composition of a cell

As indicated in Section 1.4.1 and 1.4.2, the band edge diagram is a useful tool for selecting suitable candidate materials for PEC cells. One such diagram is reported in Fig. 1.3, showing various material's band edges together with the water reduction/oxidation potential. Few materials satisfy requirements 1 and 3 of Section 1.4.1. For example, SiC, ZnO, and TiO_2 all satisfy requirement 1 while presenting a bandgap exceeding the set threshold of 3.1 eV.

On the other hand, many materials satisfying both requirements are often unstable. Ta_3N_5, which presents a high theoretical efficiency but is prone to photocorrosion due to the creation of surface states created by the displacement of nitrogen by

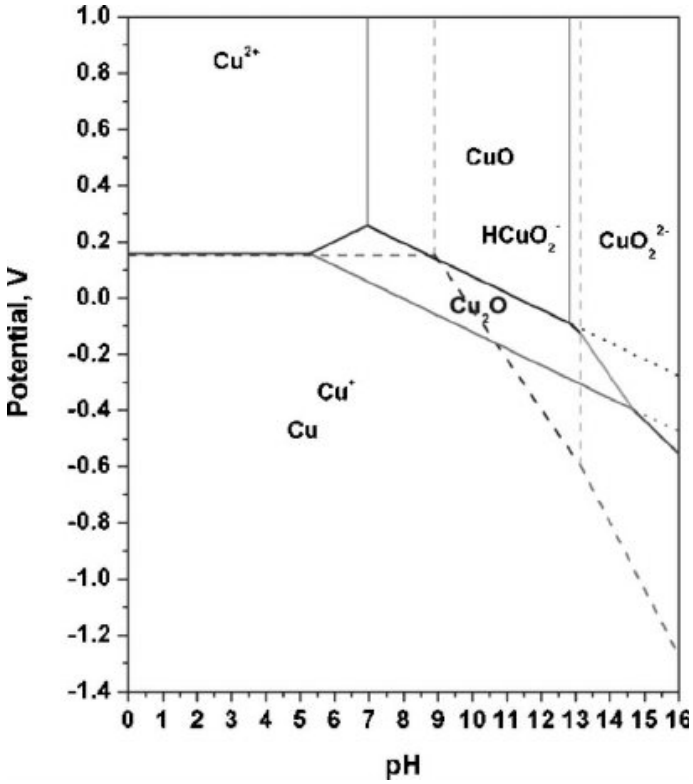

Figure 1.4: *Pourbaix diagram of Cu in aqueous solution at 25 degrees Celsius. Reproduced from Ref. [22], © The Electrochemical Society. Reproduced by permission of IOP Publishing Ltd. All rights reserved*

oxygen atoms [19]. This, coupled with its difficult synthesis, makes it a challenging material to use for PEC cells. CdS also presents a favorable bandgap while being subject to photocorrosion [20]. Together with its toxicity [21], this criticality renders the use of CdS cells for PEC applications difficult. Many other materials present a bandgap compatible with the aforementioned requirements, and each has its own criticalities.

Cu_2O, the material subject of this study, is one having the necessary bandgap for water-splitting applications, but like all the previously analyzed materials, Cu_2O also presents some criticalities. It too is known to be susceptible to photocorrosion through the photoreaction reaction [17]

$$M_xO_y + 2\,ye^- + yH_2O \overset{\text{electrolyte}}{\rightleftharpoons} xM_{(s)} + 2\,yOH^-_{(aq)}$$

Cu_2O also has a relatively small stability window when in aqueous environment, as may be seen from its *Pourbaix diagram* in Figure 1.4, a plot of possible thermodynamically stable phases in aqueous solution. Besides the required band edge positions, Cu_2O presents many advantages that make its analysis worthwhile: it is non-toxic, abundant, low cost, and has the potential to have a high photocatalytic activity.

The metal-counter electrode configuration used to study PEC cells in this chapter is just one of the possible configurations. Other possibilities include the biasing of the photocathode/photoanode with a p-n junction in a monolithic device and the simultaneous use of photocathode/photoanode, which allows to address the bandgap

requirement. This is because by using a tandem system photoanode/photocathode, each electrode only needs a bandgap compatible with "its" half-reaction. In this case the two bandgaps need to be compatible so that the excited electrons from the photoanode can migrate to the photocathode. This is translated in the requirement that $E_C^{anode} > E_V^{cathode}$.

To increase performance, the use of *nanostructured electrodes* is also a possibility. Here different morphologies allow for an increase in surface area, a shorter diffusion path, and the occurrence of quantum size effects.

A conducting substrate known as a *back-contact* is needed when constructing thin-film samples. These are usually chosen to be transparent since this allows for illumination from the back of the sample. Some examples of such materials are F-doped SnO_2 (FTO), Sb-doped SnO_2 (ATO), Sn-doped InO_3 (ITO), and Al-doped ZnO (AZO). To ensure no disruption of the current flow the back-contact should form an Ohmic junction with the material. The formation of an Ohmic (as opposed to a Schottky) contact can be verified by the analysis of each material's work function (the minimum energy to remove an electron from the material at 0 K, $E_{vacuum} - E_F$). For n-type photoanodes, this requires conducting materials with a work function that is lower than that of the photoanode itself. The use of the work function to determine the type of junction formed is not always accurate, as some materials like Cu_2O are expected to have a Schottky junction with FTO but have been measured to form an Ohmic junction instead [23]. This is the case for the back-contact used in this study.

Different materials can be laid on the semiconductor to enhance the performance of a PEC cell. Three types of layers are important for this study.

- Passivation layers: these are composed of chemically stable materials that are laid on top of the semiconductor to increase its chemical stability. This is achieved by preventing direct contact of the semiconductor with the solution, preventing corrosion phenomena. Some examples include TiO_2, and NiO.
- Electron/hole extraction/transport layers: layers with a band position relative to the absorber which allows for the passage of a type of charge carries but not the other, avoiding recombination. Examples are FTO, ITO, and graphene.
- Reaction catalysts: materials aiding the reaction by modifying its kinetics. Examples are IrO_2, Pt, RuO_2, and cobalt-based catalyst.

To be viable options all these materials need to be transparent (in the wavelength window of interest for the photoelectrode), stable, and need not to reduce excessively the charge transport efficiency.

Experimental instrumentation

In this chapter, an overview of the physics and role of different instruments for PEC research is given. The specific instruments used in the analysis carried out in the next chapter are then discussed.

2.1 Reference electrode

To characterize the behavior of an electrode, a direct measurement of the solution-electrode potential is not possible. This is because any measurement instrument used for this goal would itself form a junction with the solution (and the electrode to be studied), introducing a dependence on the apparatus. The two-electrode configuration used until now is also not suited for the characterization of a single electrode when current passes through the circuit. The presence of a current implies potential drops across the resistances of the circuit, making the decoupling of information about the electrode from that of the cell very difficult.

For this purpose, a three-electrode setup is used. Two electrodes, the *working electrode* and *counter electrode*, are placed in the solution and current is allowed to run through them. A third electrode, the *reference electrode*, is also inserted in the solution, and the potential difference between the reference and working electrodes is monitored. The setup is built to have little to no current passing through the reference electrode, effectively decoupling the measurement from the apparatus. In this way, measurements like the electrode's I-V characteristics can be obtained. To obtain information about the working electrode, the reference must have a stable and known Nernst potential difference with the solution. There exist many possibilities for a reference electrode, in this work a silver/silver chloride electrode in saturated KCl was used.

2.2 Potentiostat

The potentiostat is a central component in the analysis of PEC cells. A simplified diagram of its inner components is shown in Figure 2.1. Most potentiostats have three test leads to be connected to the cell. These are to be connected to the working (WE), counter (CE), and reference (REF) electrodes. A fourth lead, not always present, is to be connected to a second reference electrode, used to "sense" the potential of the working electrode. It is indicated as SENSE, and when no second reference electrode is present it is to be connected to the WE. The purpose of a potentiostat is to measure the potential difference between the REF and the

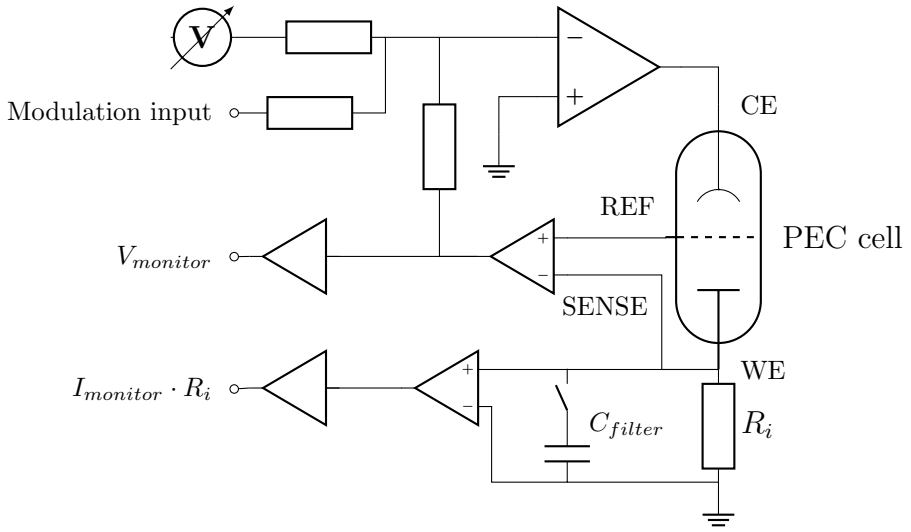

Figure 2.1: *Simplified diagram of a potentiostat connected to a PEC cell*

SENSE, making sure that it stays equal to the desired potential by adjusting the potential at the CE. The desired potential is the potential set by the user plus the potential present at the modulation input.

The REF and SENSE inputs draw negligible current. This means that the entire current flowing through the cell passes through the *current range resistor* (R_i in the figure), which converts it into voltage. The value of the resistor is often chosen to have a potential difference of 1V when the current is at the maximum of the range. In parallel a capacitor is found. Its value can often be selected (or the capacitor outright disconnected). The capacitor and resistance in parallel form an RC filter, reducing noise and giving a more stable measurement. An Autolab PGSTAT 204 potentiostat was used for the following analysis.

2.3 Scanning electrochemical flow cell

The scanning electrochemical flow cell is an advanced electrochemical setup that couples a flow cell, where the electrolyte is continuously fluxed through the cell from a reservoir, with an XYZ locomotion system. The flow helps remove bubbles of hydrogen or oxygen sticking on the electrodes after formation and enhances the transport of species to or away from the electrodes. The possibility to move the cell allows the study of inhomogeneous samples.

To illustrate the advantages, a useful example is that of the study of the dependence of a physical property on the thickness of a certain layer applied to the sample. Using the classical analysis methods, various samples all with different thicknesses have to be prepared, and each has to be then analyzed separately. The number of "experimental points" is then limited by the number of samples the researcher can prepare (itself often dictated by the available *time*). By using a scanning flow cell, only one sample presenting a gradient of that layer's thickness is needed. Besides, only one measurement needs to be made, instructing the cell to move at different coordinates during the data collection. The number of different points obtainable is now limited by the area of the sample studied at each iteration. In the cell used for

this work, the measurement area had a circular area with a diameter of 1.5 mm.

The specific flow cell used in this study was built domestically. The frame of an Ender 5 Pro 3D printer was used as the starting skeleton of the system. The XYZ positioning system uses 3 stepper motors, two of them driving the belts moving the sample plate on the XY plane, and one moving the photo-electrochemical cell along the Z axis by rotating a screw. After the correct XY placement is reached, the cell is lowered onto the sample by the Z controller. To establish when the cell has made contact with the sample a pressure sensor is used, monitoring the pressure that the cell is exercising on the sample until a threshold is passed. The plate presents apertures to allow the retro-illumination of the samples. The electrochemical cell was 3D printed out of durable and inert resin. It presents 5 openings: 2 for the electrolyte tubes, 2 for the working and counter electrodes, and one for illumination from above. The electrolyte is moved by a peristaltic pump, which constantly moves it from the reservoir to the cell and back. A second pump can pinch the inlet tube to help remove bubbles that could have been introduced in the canal of the cell while the cell was raised. The reservoir can be fluxed with inert gas (argon). All the electronics are managed by an Arduino Mega, which communicates through several digital inputs and outputs with the potentiostat and with a Thorlabs THORLABS DC2200 LED driver, and custom LabView software.

A typical automated measurement sequence consists of:

1. XY movement to the desired coordinate
2. Z approach until desired pressure is reached
3. bubble removal by pinching the inlet tube
4. potentiostat performs photoelectrochemical measurements
5. cell lifts and the process starts back from 1.

2.4 Sample preparation

The samples studied with the aid of the flow cell presented in Section 2.3 are composed of thin layers of material laid on a conductive and transparent back-contact (see SubSection 1.4.3). The back-contacts are often bought looking for the required parameters, and the sample materials are laid upon them. Various methods exist to achieve the deposition of thin layers of materials, in this section, some of the more common methods are illustrated.

2.4.1 Sputtering

Sputtering, intended as sputter deposition, is a high-vacuum coating technique belonging to the group of physical vapor depositions. It is based on the principle of using the energy of a plasma (a highly ionized gas) to pull atoms of the wanted material (the cathode) and deposit them onto the substrate. The operating pressures of this technique are high, usually 10×10^{-1} to 10×10^{-3} mbar. Still, it is necessary to start at lower pressures (10×10^{-5} to 10×10^{-7} mbar) to evacuate most of the other

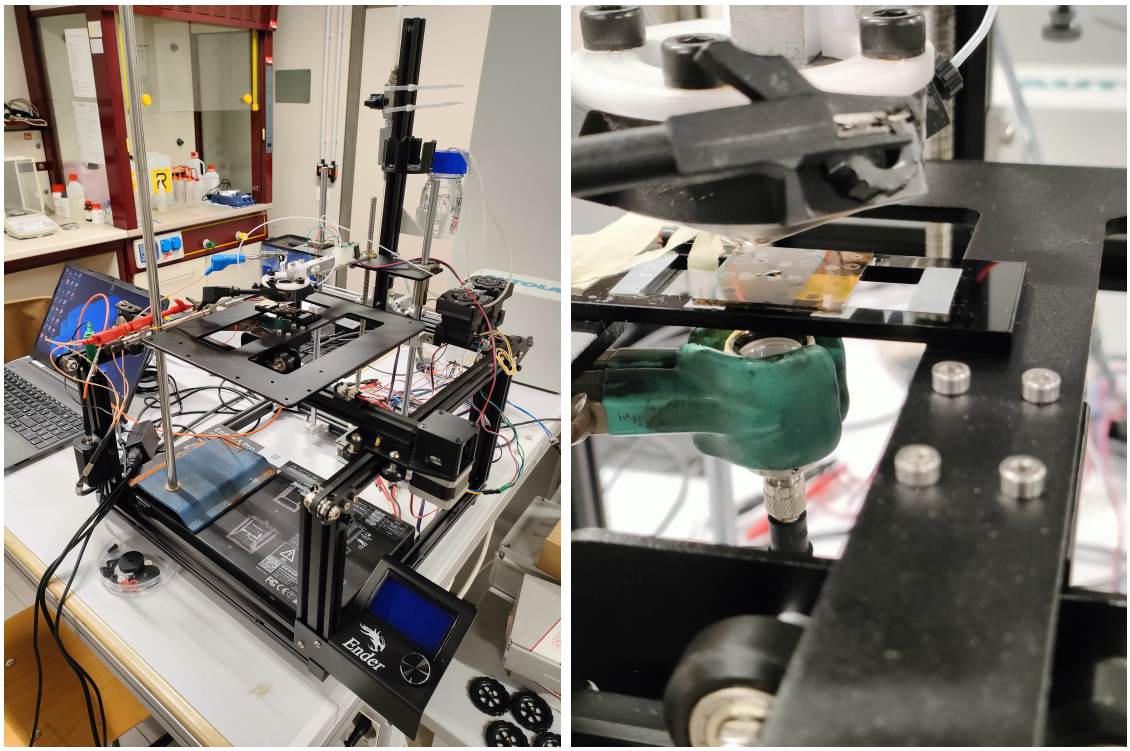

Figure 2.2: *Left: Scanning electrochemical flow-cell used for the data analysis. Right: close-up of the analyzed sample after the measurements*

gasses, to avoid contamination (especially oxygen). The gas used for this purpose is a pure and inert gas, usually argon.

There are various ways to impart energy to the gas and to direct the ions toward the target, some examples include:

- Direct current (DC) sputtering: an ion plasma is ignited by applying a DC voltage between the cathode and the substrate of 500 to 1000 V. These ions then accelerate toward the cathode, imparting the cathode's atoms their momentum and allowing them to detach, thus beginning the sputtering. With this technique, only electrical conductors can be sputtered, since for insulators an opposing electrical field builds up as charges accumulate in the material, stopping the process.

- Radio frequency (RF) sputtering: a high-frequency alternating field is applied with an offset negative potential on the target. The alternating field accelerates the ions and electrons in both directions. For argon, at around 50 kHz, the ions start lagging behind the field notably, due to their smaller charge-mass ratio. The electrons keep oscillating and this results in a high plasma rate. The ions are then accelerated toward the target by the offset potential. This technique also allows for the sputtering of insulators and semiconductors.

- DC triode sputtering: the target is placed outside the plasma chamber as a third electrode. In this way, plasma generation and sputtering are decoupled.

- Magnetron sputtering: in addition to the electric field used in the preceding techniques, a magnetic field is created behind the cathode plate. Due to this

Material	Argon flux (standard cm^3/min)	Pressure (mbar)	Power (W)	Mode
AZO	7	2×10^{-3}	40	RF
TiO_2	10	8×10^{-3}	40	RF
NiMo	10	8×10^{-3}	20	DC

Table 2.1: Parameters of the sputtering setup used for the deposition of each material. These were used for both the calibration and the deposition on Cu_2O

Material	Deposition time (min)	Thickness (nm)	Sputtering rate (nm/min)
AZO	120	239	2
TiO_2	480	81	0.17
NiMo	360	580	1.6

Table 2.2: Data from the calibration of the sputtering rate of different materials on silicon. The thickness of the layers is obtained from Fig. 2.4. The obtained rates are considered equal to the rates on Cu_2O

field, the charge carriers (electrons) are deflected into cycloid orbit, prolonging their path near the target surface and thus raising the number of impacts, increasing the plasma density in the region above the cathode. The created ions are hardly affected by the magnetic field due to the low charge-mass ratio and thus impact the cathode predominantly underneath these areas of high plasma density. This creates the characteristic erosion trenches in the target material typical of magnetron sputtering.

- Reactive sputtering: reactive gasses like O_2 or nitrogen are introduced in the sputtering chamber together with argon. These gasses react with the sputtered atoms to form new compounds, which are then deposited onto the substrate.

The sputtering setup shown in Figure 2.3 was used for the analysis in the following chapter. Since sputtering is a non-directional depositing technique, the sputtered atoms come to rest on any free surface. This results in the various colors observed on the chamber walls, which are layers of previously deposited materials. In this work, magnetron sputtering was used to deposit the Aluminum-doped Zinc Oxide, Titanium dioxide, and Nickel-Molybdenum (NiMo) layers. The sputtering parameters used for each material are shown in Table 2.1

To establish the sputtering rates of each material a wafer of crystalline silicon underwent sputtering for a set amount of time. The obtained sample was then sliced and analyzed in a scanning electron microscope to determine the layer's thickness. The measurement pictures are reported in Fig. 2.4, while the calibration data is found in Table 2.2. By considering a constant sputtering rate, the thickness of the materials laid next can be inferred.

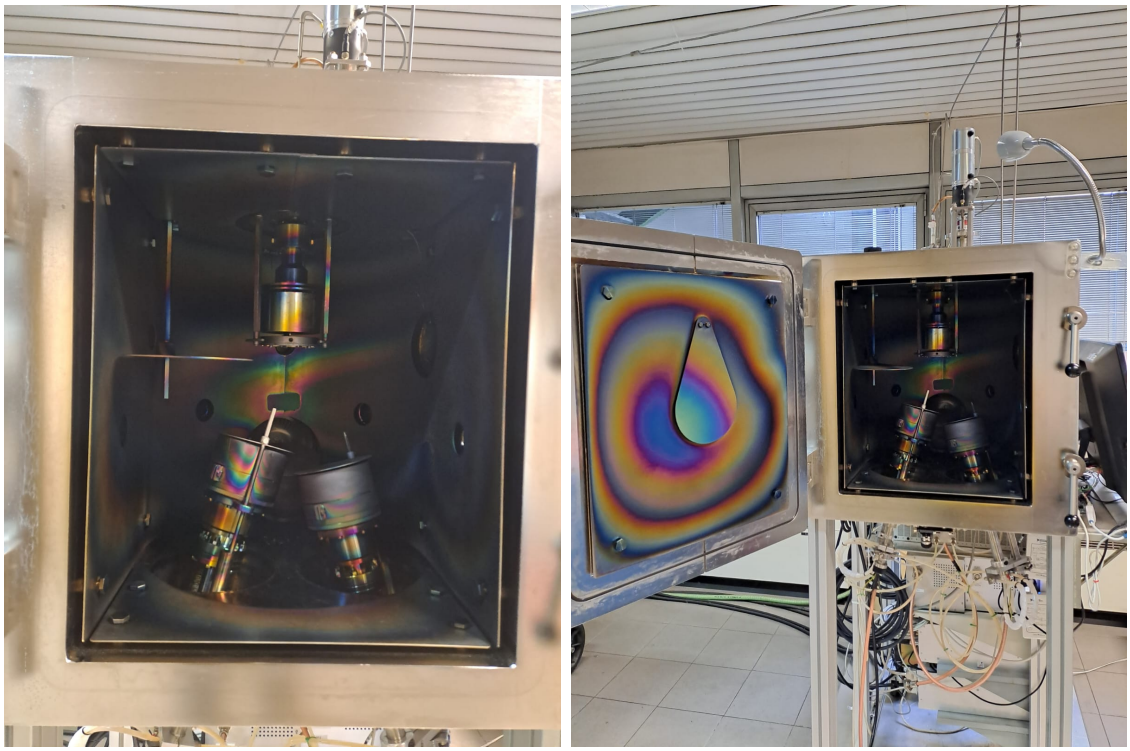

Figure 2.3: *Magneton sputtering chamber used. It presents 3 possible cathode sites (at the bottom of the chamber) and a multiple sample holder (at the top of the chamber)*

2.4.2 Spray pyrolysis

In spray pyrolysis, a thin film is deposited by spraying a precursor solution on a heated surface, where the constituents react to form a chemical compound. The reactants are chosen so that any product other than the desired one is volatile at deposition temperatures. Typical spray pyrolysis equipment consists of an atomizer, a temperature controller and a substrate heater. The main atomizers used are air blast, ultrasonic, and electrostatic. It is used predominantly to prepare dense and porous oxide films, ceramic coatings, and powders. In this work spray pyrolysis was used to deposit the Cu_2O photocathodic layer.

2.4.3 Electrodeposition

Electrodeposition, also called electroplating, is a technique in which a film of solid metal or oxide is deposited onto the surface of conducting materials by electrochemically reducing the desired metal ion or its chemical complex present in the solution. The physical principles on which this deposition technique is based are those discussed in Section 1.2. The system is effectively an electrochemical cell, where the reduction reaction at the cathode is used to deposit the wanted material on the conductive cathode. Varying factors like the type of voltage applied to the cell (e.g. pulse electroplating), the geometry of the disposition of the samples (like in barrel electroplating), the introduction of different components to the cell (e.g. brush electroplating), etc., it is possible to tune the desired characteristic of the film.

This technique is cost-effective and has a high deposition rate, but the limitations on the possible materials for deposition, the little control over the thickness of the deposited layer, and the high cleanliness required of the surface make it suitable for low precision samples.

2.5 Scanning electron microscope (SEM)

When studying thin layers, a scanning electron microscope is an essential tool. This instrument produces images of a sample by scanning the surface with a focused beam of electrons that are originated, focused, and directed from inside the *column*. The electrons interact with the sample's atoms, producing various signals containing information on the topology (and composition) of the material.

Typically, electrons are produced in the column by an electron gun. For this study, thermionic emission was used, where a metal (tungsten) filament is heated at high enough temperature that the electron's kinetic energy allows them to leave the surface of the material. The electron beam then passes through one or two condenser lenses to obtain a spot with a diameter in the order of the nanometer. The beam is then deflected by pairs of scanning coils (or deflector plates), which move it in a *raster* fashion over a rectangular area of the sample's surface.

The electrons interact with the sample, losing energy by random scattering and absorption. This interaction results in the emission of high-energy electrons by elastic scattering (back-scattering), secondary electrons by ionization of the atoms on the sample, and electromagnetic radiation. Based on the type of signal, different technologies and detector positions have to be used.

The energy of the electrons determines their mean free path in solid matter. The high-energy electrons emerging from elastic scattering can travel further through the material, thus on average originating deeper in the sample. On the opposite, electrons originating by ionization are lower in energy and thus emerge from a few nanometers under the sample surface, and are thus of interest to determine the topology of the sample's surface [24]. The originated secondary electrons are attracted toward an electrically biased grid and then further accelerated toward a scintillator-photomultiplier system. The intensity of the detected beam is represented as the grey scale value of the pixel corresponding to the position of the sample where the beam was deflected. By moving the beam across the surface of the sample the final image is composed.

The back-scattered electrons and the electromagnetic radiation (often X-rays) emitted are still of interest, mainly in analytical SEMs. This is due to the dependence of their intensity on the atomic number of the material being analyzed. In this work, a CAMBRIDGE STEREOSCAN 360 SEM was employed using a 20 kV column potential and 30 pA incident current on the sample. The images in Figure 2.4 were taken through its use.

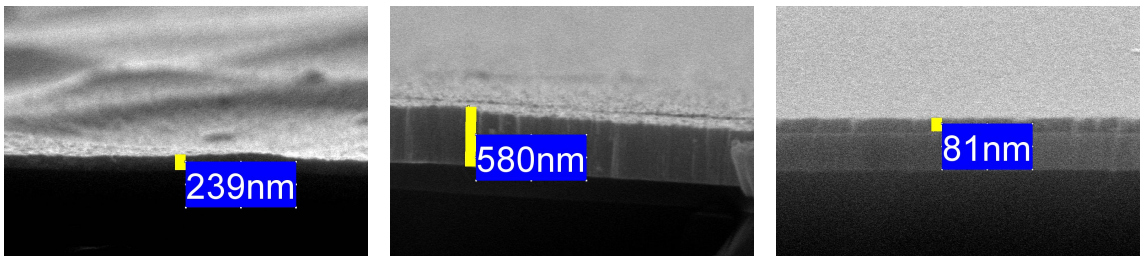

Figure 2.4: *Images from the calibration of the sputtering rates for AZO (left), NiMo (center), and TiO_2 (right). All these were laid on crystalline silica*

Study of a Cu_2O half-cell

3.1 Preparations

The sample was produced by the Austrian Institute of Technology through spray pyrolysis. Three test pieces were made, laying a thin coating of the wanted material upon an FTO back-contact, itself placed on glass. Each sample was made from copper oxides, presenting Cu_2O, CuO, and a sample made from a combination of both. The following analysis has been conducted on Cu_2O as a photocathode. The objective of the study was to analyze the behavior of the sample after selected materials were placed upon the Cu_2O layer through sputtering.

The chosen materials to place on top of the sample were:

- TiO_2, a wide-band, chemically stable material used as a buffer between the sample and the electrolyte to prevent photocorrosion.
- Al-doped ZnO (AZO), which is a transparent and conductive layer. In this context, it is employed as an electron transport layer that due to its band edges' position relative to the ones of Cu_2O accepts the electrons photogenerated in the active layer, but not the holes. It's also n-doped by the addition of Aluminum to improve the electron's conductivity and worsen the holes'.
- NiMo, an alloy containing 80 % of nickel and 20 % molybdenum, which is known to be a good catalyst for hydrogen evolution reactions. The molybdenum is introduced because the sole nickel, being ferromagnetic, would mask the magnetic field of the magnetron sputtering, thus lowering the sputtering yield.

To test the behavior of each layer in different configurations a set of masks was cut from inert plastic using a laser cutter, and successive depositions through sputtering were performed. The deposition procedure, together with a picture of the sample, is schematically reported in Fig. 3.1, while the thicknesses of the deposited layers are reported in Table 3.1. Each zone was then tested using the scanning electrochemical flow-cell described in Section 2.3. Where illumination of the sample was required a 385 nm LED was employed.

The choice of the electrolyte was dictated by the window of stability of Cu_2O based on pH. By looking at its Pourbaix diagram, reported in Figure 1.4, it can be seen how Cu_2O is stable at pH between 5.5 and 15.

Following this constraint, an alkaline electrolyte was chosen to ensure also the stability of the catalyst layer (NiMo) [25], which had been experimentally assessed by the research group in the past. The selected pH was 11. To achieve this, a buffer

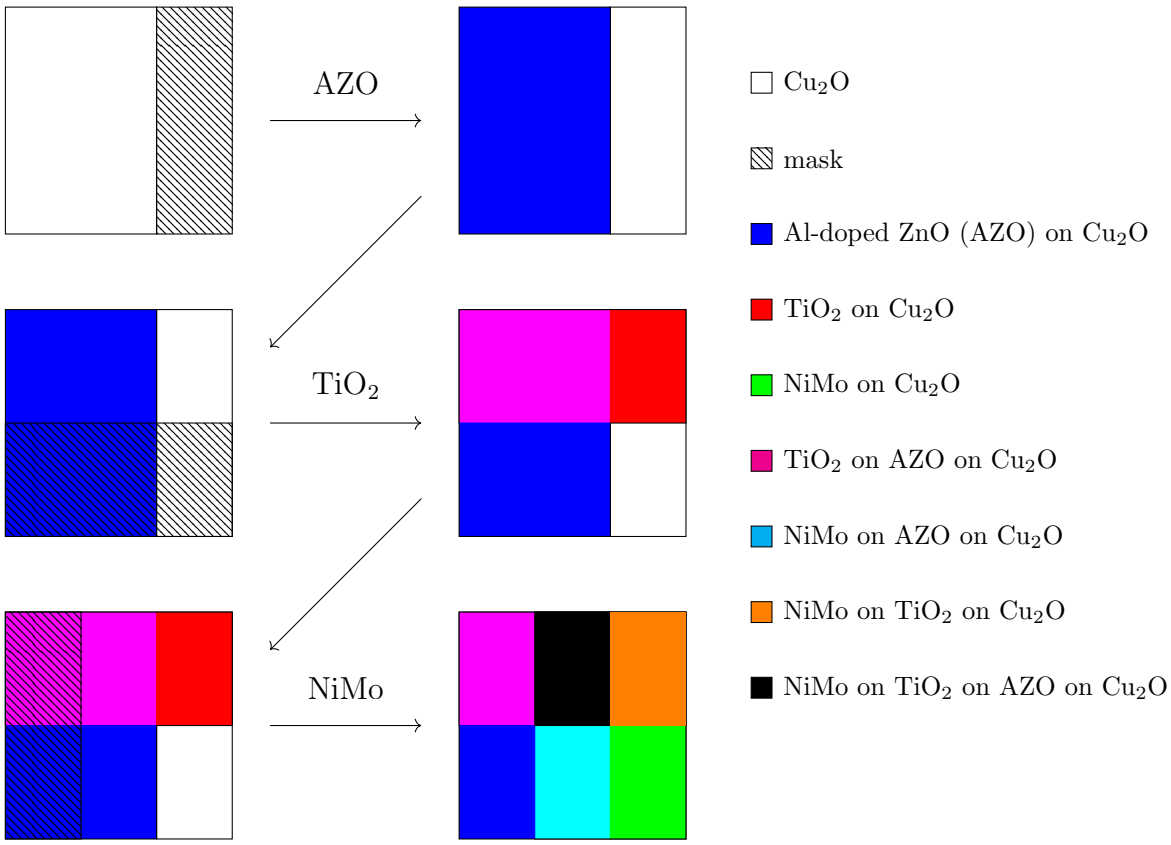

Figure 3.1: *On the top: schematics of the puttering sequence of the sample. The material represented by each color is indicated in the legend. Bottom-left: samples placed on the sputtering sample holder. Bottom-right: close-up of the analyzed sample*

Material	Deposition time (min)	Sputtering rate (nm/min)	Thickness (nm)
AZO	30	2	60
TiO_2	48	0.17	8
NiMo	10	1.6	16

Table 3.1: *Sputtering data for the various layers on the sample. The sputtering rate was taken to be equal to that of the calibration, as indicated in SubSection 2.4.1*

solution of borate buffer 0.25 M was used. The solution was assembled by making an aqueous solution of boric acid 0.25 M and adding droplets of high-concentration NaOH solution (4 M) until the desired pH was reached. Na_2SO_4 was added up to a concentration of 0.5 M as a dissociating inert salt to improve the conductivity of the solution. To ensure competition with molecular oxygen dissolved in the solution (which can "steal" photogenerated electrons from the hydrogen reduction reaction), argon gas was constantly fluxed through the electrolyte.

3.2 Experimental measurements

3.2.1 Chronoamperometry

The graphs of the data obtained by the analysis are reported in Fig. 3.2. Note the different y-axis scales. The measurement was performed using *chopped-light*, i.e. turning the LED light on for one second and off for the successive. This can be better seen in the graph of NiMo on TiO_2. When the light is turned on, the current increases in absolute value (being a photocathode the current and its increase are *negative*). The difference in current when the light is on and when it is off is called *photocurrent*.

From the graphs, it is possible to note the *transient* behavior of the system when the light is turned on/off. This transient is due to the total capacitance of the cell, given by the electrical double layer at the interface and by the other charge layers (the contribution of which is less marked).

The performance of all the samples is underwhelming, showing a photocurrent in the order of the µA. Among all the sample's configurations, NiMo on TiO_2 shows the best performance, one order of magnitude greater than the others (but still in the tens of µA).

3.2.2 Data refinement

Due to the low photoproduced currents, the behavior of the Cu_2O photocathode under the chopped illumination is hidden by noise. To better illustrate the sample's behavior a *moving average* of the data was taken, obtaining the graphs reported in Fig. 3.3. For each point, this consisted of taking the average of the 5-point neighborhood and using it as the new data point.

The trend in photocurrent may contain valuable information regarding the chemical stability of the electrode. To extrapolate the trend in photocurrent, the *sta-*

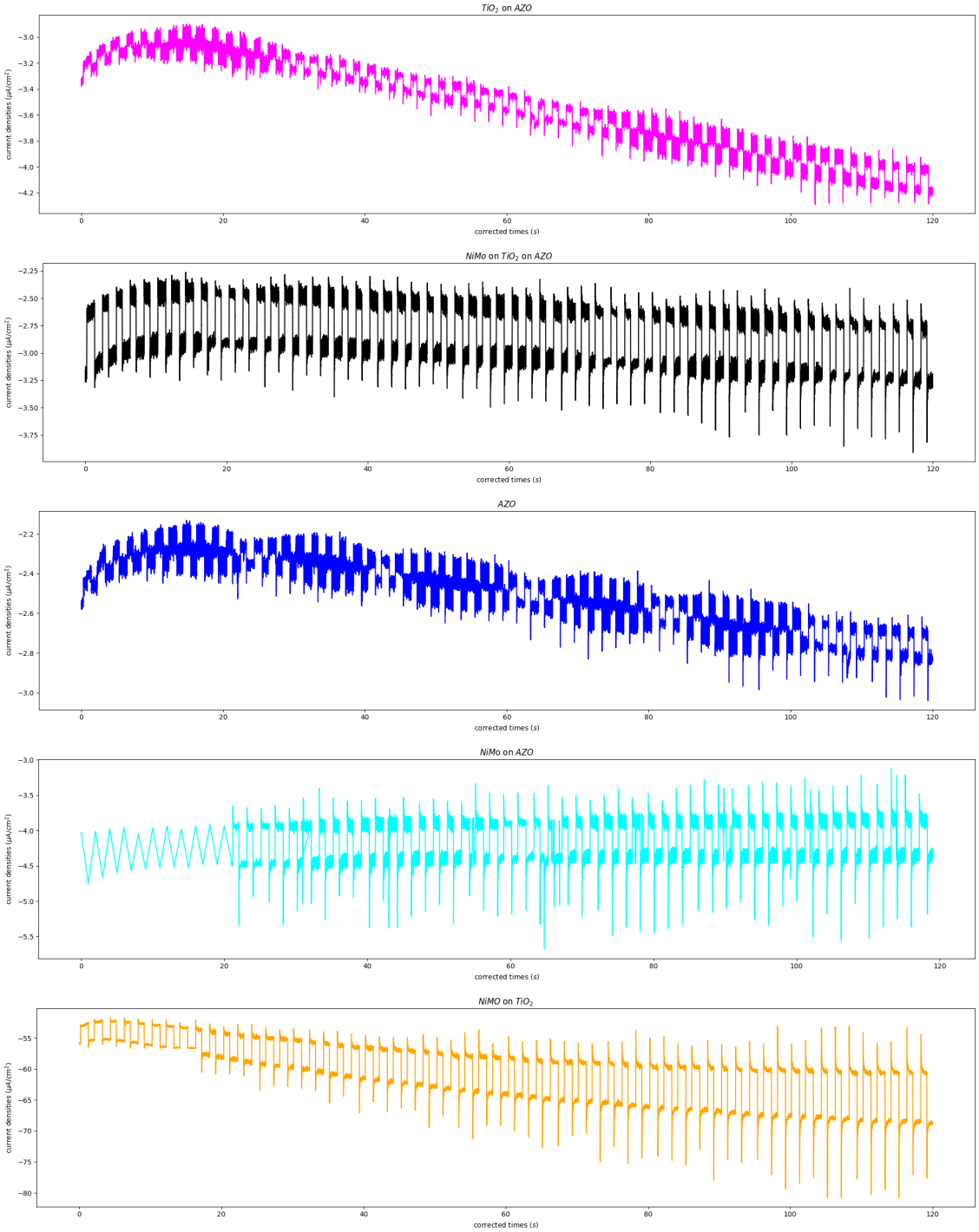

Figure 3.2: *Graphs of the data obtained from the chronoamperometry for the different sections of the samples. "corrected time" stands for the time elapsed from the start of the chronoamperometry*

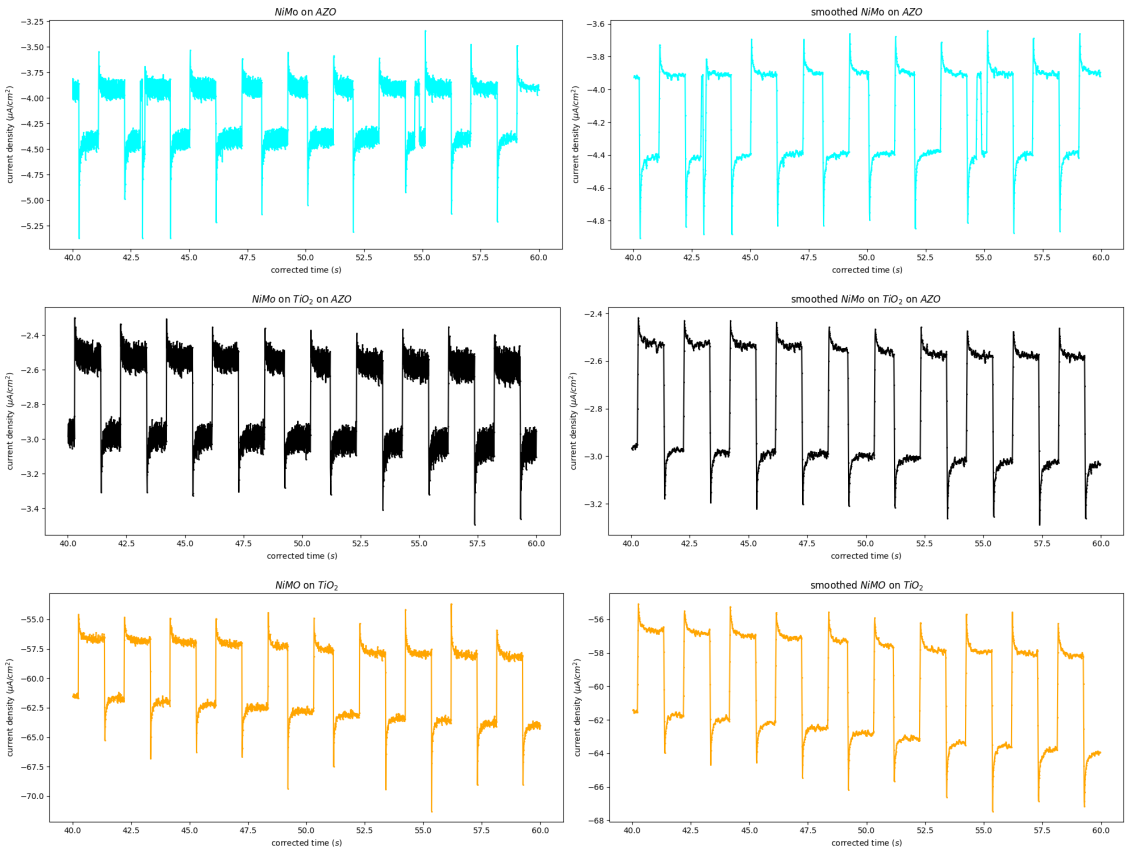

Figure 3.3: *Graphs of the chronoamperometry's data smoothed through the use of a moving average. On the left is the raw data and on the right is the smoothed data. For each section of the sample a window of 20 seconds was selected to better illustrate the result*

tionarity of a state of the electrode needs to be defined. To do this the standard deviation of a group of six cells around a time point was calculated and plotted, one example is given in the top-left of Figure 3.4. Through this plot, an optimal standard deviation was chosen to identify the stationary states of the chronoamperometry. The difference in the (average) current between the stationary states was then computed, plotted, and fitted, the result shown in Figure 3.4. None of the analyzed configurations present a downward slope associated with the degradation of the electrode.

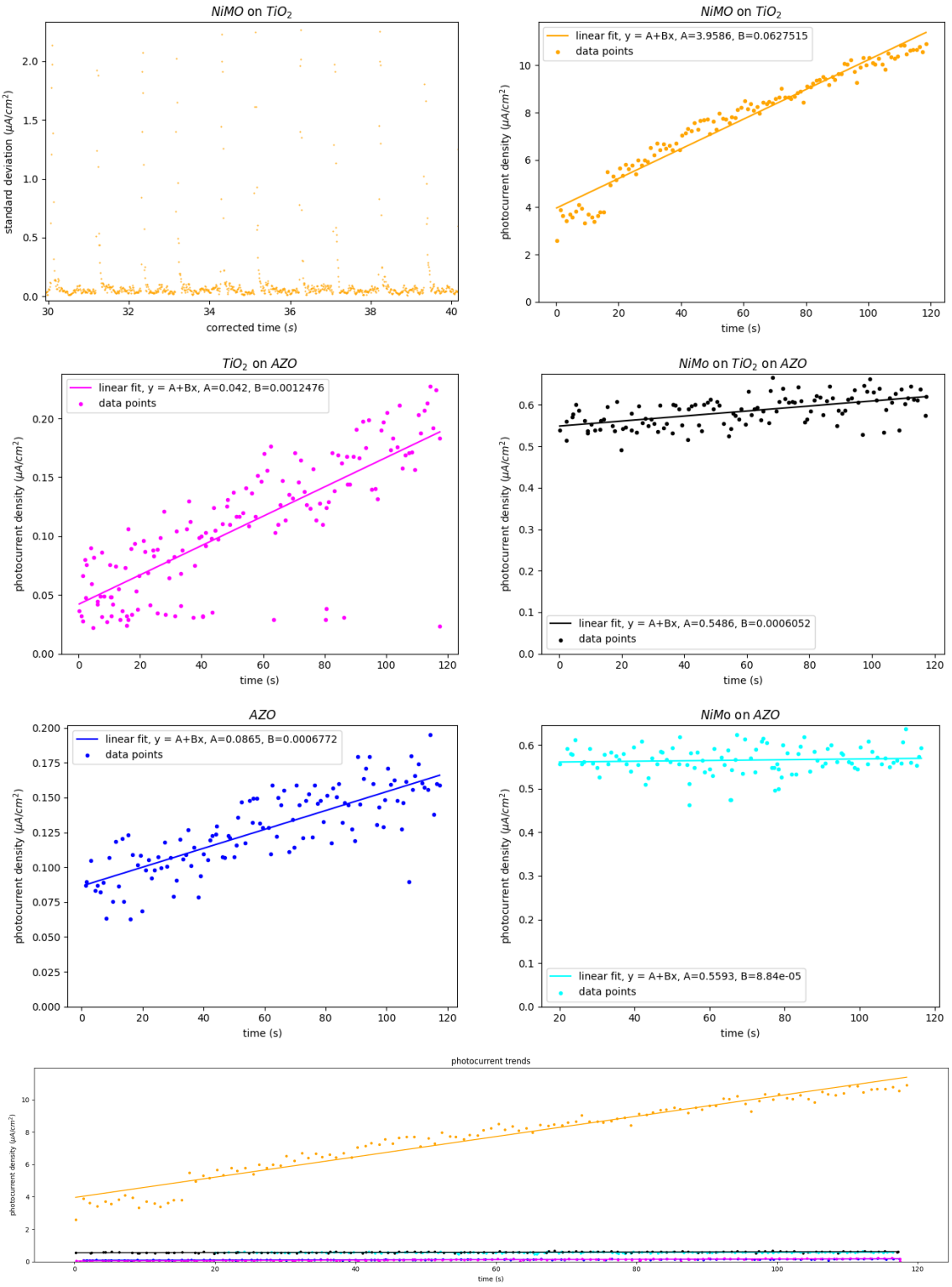

Figure 3.4: *Top-left: 10-second window of the standard deviation plot for a 6-point neighborhood. In this case the threshold standard deviation was taken to be 0.2 $\mu A/cm^2$. From top-right to third row-right: linear regressions of the measured photocurrent as a function of time. Bottom: all photocurrent trends plotted together*

Conclusions

4.1 Sample performance

The Cu_2O sample, fabricated by the Austrian Institute of Technology through spray pyrolysis, was modified by adding a TiO_2 passivation layer, a AZO electron transport layer, and a NiMo catalyst layer. The sample was then studied as a photocathode in a high throughput scanning electrochemical flow cell.

When illuminated with a chopped 385 nm LED light, the sample presented a photocurrent. By analyzing the graphs for each deposition configuration, NiMo on TiO_2 presented the best performance both in terms of generated photocurrent and stability.

NiMo on TiO_2 photocurrent density was around 10 µA/cm^2. This is quite small compared to those found in the literature, attesting around 0.1 to 5 mA/cm^2. This low photocurrent is likely due to the absence of a well-engineered hole transport layer between the Cu_2O film and the FTO substrate, resulting in strong recombination at the back contact. Therefore, future studies will be repeated on a different architecture of the photocathode employing an additional interlayer to boost photocurrent. Nevertheless, the experimental protocol applied in this work proved to be effective and time-efficient, and will be utilized for future investigations.

4.2 Future perspectives

While this particular sample does not present the required characteristics for efficient hydrogen production, the study hints at the usefulness of protective and catalytic layers applied to the surface. Future studies may include different deposition techniques, new deposited materials for protection/catalysis, and the insertion of the aforementioned hole transport interlayer between the Cu_2O and the FTO substrate.

The optimal thickness of the various layers could be studied. For this purpose, the setup used in this analysis could play a big role. By sputtering a variable thickness layer of each material on a Cu_2O sample (by for example keeping the sample at a fixed angle with respect to the sputtering source), the performance of different thicknesses could be analyzed at once.

The Cu_2O parameters could also be studied and optimized: thickness, compactness, structure, etc.

The potential benefits of a viable PEC cell for hydrogen production alone make for a strong incentive towards deeper research into the field. While photovoltaic-electrolysis systems seem more and more viable for the world's hydrogen objectives, research in PEC is deeply tied to advances in other fields like nanotechnology, material science, optics, etc. Any advance in these fields influences PEC research, and vice-versa, making the prospect of new techniques and technologies a reality.

Bibliography

[1] Global Monitoring Laboratory. *trends in CO_2*. Tech. rep. National Oceanic and Atmospheric Administration, 2024. URL: https://gml.noaa.gov/ccgg/trends/.

[2] William D. Collins et al. *Global Climate Projections*. Tech. rep. International Panel on Climate Change, 2007.

[3] Alessandro Bottin. *Un Pianeta In Pericolo*. AltroMondo Editore, 2024.

[4] Bongani Thusi et al. *World Energy Resources, 2013 Survey: Summary*. Tech. rep. World Energy Council, 2013.

[5] Nathan S. Lewis and Daniel G. Nocera. "Powering the planet: Chemical challenges in solar energy utilization". In: *Proceedings of the National Academy of Sciences of the United States of America* (2006).

[6] N S Lewis et al. *Basic Research Needs for Solar Energy Utilization. Report of the Basic Energy Sciences Workshop on Solar Energy Utilization, April 18-21, 2005*. Tech. rep. U.S. Department of Energy, Apr. 2005. DOI: 10.2172/899136. URL: https://www.osti.gov/biblio/899136.

[7] International Energy Agency. *Ammonia Technology Roadmap*. Tech. rep. IEA, 2021.

[8] International Energy Agency. *Global Hydrogen Review 2023*. Tech. rep. IEA, 2023.

[9] Muhammad R. Usman. "Hydrogen storage methods: Review and current status". In: *Renewable and Sustainable Energy Reviews* 167 (2022), p. 112743. ISSN: 1364-0321. DOI: https://doi.org/10.1016/j.rser.2022.112743. URL: https://www.sciencedirect.com/science/article/pii/S1364032122006311.

[10] R. J. Detz, J. N. H. Reek, and B. C. C. van der Zwaan. "The future of solar fuels: when could they become competitive?" In: *Royal Society of Chemistry* (2018).

[11] W.A. de BSc Jong. "PEC versus PV - E A Future Potential Comparison". MA thesis. Utrecht University, 2018.

[12] Hydrogen and Fuel Cell Technologies Office. *Multi-Year Program Plan*. Tech. rep. U.S. department of energy, 2024.

[13] Renato Cozzi, Pierpaolo Protti, and Tarcisio Ruaro. *Elementi di analisi chimica strumentale*. Scienze Zanichelli, 2013.

[14] V. S. Bagotzky. *Fundamentals of Electrochemistry*. Plenum, 1993.

[15] Nicolae Goga et al. “A Review of Recent Developments in Molecular Dynamics Simulations of the Photoelectrochemical Water Splitting Process”. In: *Catalysts* 11.7 (2021). ISSN: 2073-4344. DOI: 10.3390/catal11070807. URL: https://www.mdpi.com/2073-4344/11/7/807.

[16] M.F. Weber and M.J. Dignam. “Splitting water with semiconducting photoelectrodes—Efficiency considerations”. In: *International Journal of Hydrogen Energy* 11.4 (1986), pp. 225–232. ISSN: 0360-3199. DOI: https://doi.org/10.1016/0360-3199(86)90183-7. URL: https://www.sciencedirect.com/science/article/pii/0360319986901837.

[17] Roel van De Krol and Michael Grätzelm. *Photoelectrochemical Hydrogen Production*. Springer, 2011.

[18] Andebet Gedamu Tamirat et al. “Using hematite for photoelectrochemical water splitting: a review of current progress and challenges”. In: *Nanoscale Horizons* 1.4 (2016), 243–267. ISSN: 2055-6764. DOI: 10.1039/c5nh00098j. URL: http://dx.doi.org/10.1039/c5nh00098j.

[19] Yumin He et al. “Photo-Induced Performance Enhancement of Tantalum Nitride for Solar Water Oxidation”. In: *Joule* 1.4 (2017), pp. 831–842. ISSN: 2542-4351. DOI: https://doi.org/10.1016/j.joule.2017.09.005. URL: https://www.sciencedirect.com/science/article/pii/S2542435117300788.

[20] Xiaofeng Ning and Gongxuan Lu. “Photocorrosion inhibition of CdS-based catalysts for photocatalytic overall water splitting”. In: *Nanoscale* 12 (3 2020), pp. 1213–1223. DOI: 10.1039/C9NR09183A. URL: http://dx.doi.org/10.1039/C9NR09183A.

[21] Min Zhou et al. “The genome-wide impact of cadmium on microRNA and mRNA expression in contrasting Cd responsive wheat genotypes”. In: *BMC genomics* 20 (2019), pp. 1–19.

[22] Youn-Jin Oh, Gyung-Soon Park, and Chan-Hwa Chung. “Planarization of Copper Layer for Damascene Interconnection by Electrochemical Polishing in Alkali-Based Solution”. In: *Journal of The Electrochemical Society* 153.7 (2006), G617. DOI: 10.1149/1.2200288. URL: https://dx.doi.org/10.1149/1.2200288.

[23] P. E. de Jongh, D. Vanmaekelbergh, and J. J. Kelly. “Photoelectrochemistry of Electrodeposited Cu2 O”. In: *Journal of The Electrochemical Society* 147.2 (2000), p. 486. DOI: 10.1149/1.1393221. URL: https://dx.doi.org/10.1149/1.1393221.

[24] Joseph I. Goldstein et al. *Scanning Electron Microscopy and X-Ray Microanalysis: A Text for Biologists, Materials Scientists, and Geologists*. Springer, 1981. ISBN: 9780306407680.

[25] Maximilian Schalenbach et al. “Nickel-molybdenum alloy catalysts for the hydrogen evolution reaction: Activity and stability revised”. In: *Electrochimica Acta* 259 (2018), pp. 1154–1161. ISSN: 0013-4686. DOI: https://doi.org/10.1016/j.electacta.2017.11.069. URL: https://www.sciencedirect.com/science/article/pii/S0013468617324222.